

# Semiconductor Electrodes

## XLVII. A-C Impedance Technique for Evaluating Surface State Properties of n-MoTe<sub>2</sub> in Acetonitrile Solutions Containing Various Redox Couples

G. Nagasubramanian, Bob L. Wheeler, G. A. Hope,<sup>\*1</sup> and Allen J. Bard\*

Department of Chemistry, University of Texas at Austin, Austin, Texas 78712

### ABSTRACT

Measurement of the in-phase (0°) and quadrature (90°) components of a small (12 mV) a-c signal at frequencies of 1-5000 Hz imposed on the d-c potential allows the determination of the a-c equivalent circuit. Study of the a-c impedance as a function of potential and frequency permits the determination of the properties of the semiconductor/solution interface. Results of measurements on n-MoTe<sub>2</sub> in MeCN containing various redox couples spanning a wide range of redox potentials are reported. The advantages of the in-phase (0°) component for extracting properties of surface states are discussed. In the region 0.3-0.5V negative of the valence band edge, the total surface-state density is ca. 10<sup>10</sup> cm<sup>-2</sup>. The adsorption in the I<sup>-</sup>/I<sub>3</sub><sup>-</sup> system on the n-MoTe<sub>2</sub> surface in aqueous and acetonitrile solvents are compared.

Surface states, due to the abrupt discontinuity at a clean surface, were first postulated by Tamm (1) and a rigorous analysis of a more general model was given by Shockley (2). The abrupt discontinuity of the ordered crystal lattice at the surface results in dangling or unsaturated bonds, producing surface energy levels different from those in the bulk material. Interface states produced by impurities incorporated at the surface, e.g., by specific adsorption of solution species or by formation of corrosion products at the semiconductor electrode surface, also can produce localized energy levels in the bandgap of the semiconductor electrode. These energy levels in the forbidden gap can serve as reservoirs of charge at the semiconductor surface. The position of the Fermi level at the surface determines whether these energy levels are filled or vacant. The determination of the energy and density of interface states as well as the time constant associated with the exchange of charge carriers with the bulk and the capture cross section is important in understanding the behavior of semiconductors in contact with a metal or with a solution.

Indeed, the relative independence of the Schottky barrier heights of low bandgap semiconductors in contact with metals of widely differing work functions was explained by Bardeen (3) and others (4, 5) in terms of pinning of the Fermi level at the surface by a high density of surface states. A similar phenomenon has been observed in photoelectrochemical (PEC) cells where low bandgap semiconductors such as Si (6, 7), CdTe (8), and GaAs (9) exhibit a nearly constant photovoltage in contact with solutions containing a number of redox couples whose redox potentials span a potential regime much wider than the  $E_g$  of the semiconductor. Such behavior can also be explained by pinning of the Fermi level by interface states (10). Interface states can be studied by a number of optical and electrical methods. Several techniques have been developed for the measurement of interface-state properties in solid-state devices. These include measurements of (i) the isothermal dielectric relaxation current (IDRC) (11); (ii) the thermal dielectric relaxation current (TDRC) (12); (iii) the low frequency capacitance-voltage behavior (13); and (iv) the a-c conductance (14). However, the liquid electrolyte in PEC systems precludes the application of the first two methods, since meaningful results can be obtained only over a wide range of temperatures which is restricted by the liquid range of the solvent. The quasi-static low frequency capacitance technique and the a-c conductance method do not suffer this limitation, and capacitance measurements have been frequently employed to

study the semiconductor/liquid interface (15, 16). However, the capacitance technique is of limited value in studying interface states. For example, in the case of metal-oxide-semiconductor (MOS) devices the capacitance method for the determination of surface-state properties is said to suffer from the following limitations (14a): (i) The variation in the capacitance values required to find the surface capacitance, even when the frequency is increased by one order of magnitude, is very small; this leads to errors in calculating the density of surface states and their time constants. (ii) The surface-state capacitance has to be extracted from a combination of the space charge layer, surface state, and the oxide layer capacitances. Since the oxide layer capacitance is in series with the semiconductor capacitance, it determines the maximum semiconductor capacitance that can be measured. This means that surface states located near the middle of the gap cannot be identified without greatly decreasing the thickness of the oxide layer, which in turn permits tunneling of charge carriers. The picture may be further complicated by the inversion layer capacitance.

The parallel equivalent conductance ( $G_p$ ) (the in-phase component of the total admittance corrected for the space charge resistance) is more useful in characterizing interface states since one can measure directly the properties related to the capture and emission rates of charge carriers by surface states. Further, it is useful in extracting data when the surface-state density is as low as 10<sup>9</sup>-10<sup>11</sup> cm<sup>-2</sup> eV<sup>-1</sup> (14a). In addition,  $G_p$  can be used to determine the values for capture probability. Even in those cases where the quadrature signal gives a frequency independent capacitance-voltage plot, the location of surface states and their time constants can be determined from the in-phase component. If the time constant for the surface states is independent of potential, the in-phase component is related to the surface-state capacitance by the following equation (see Appendix)

$$G_p/\omega = \frac{C_{ss}\omega\tau}{(1 + \omega^2\tau^2)} \quad [1]$$

where  $C_{ss}$  is the surface-state capacitance,  $\omega$  is the angular frequency of the applied a-c signal, and  $\tau$  is the time constant associated with carrier exchange. From the relevant equivalent circuits for the interface given in Fig. 1a, it is clear that the conductance does not contain  $C_D$ , the depletion layer capacitance, but depends only on the surface-state branch of the equivalent circuit. A plot of  $G_p/\omega$  at a given potential will have a maximum value at a particular frequency; the reciprocal of that frequency yields a weighted average of the time constant associated with the surface states, when  $\omega\tau = 1$ . This leads to a maximum value in  $C_{ss}$

\* Electrochemical Society Active Member.

<sup>1</sup> Permanent address: School of Science, Griffith University, North Brisbane, Queensland 4111, Australia.

Key words: impedance, semiconductor, surfaces.

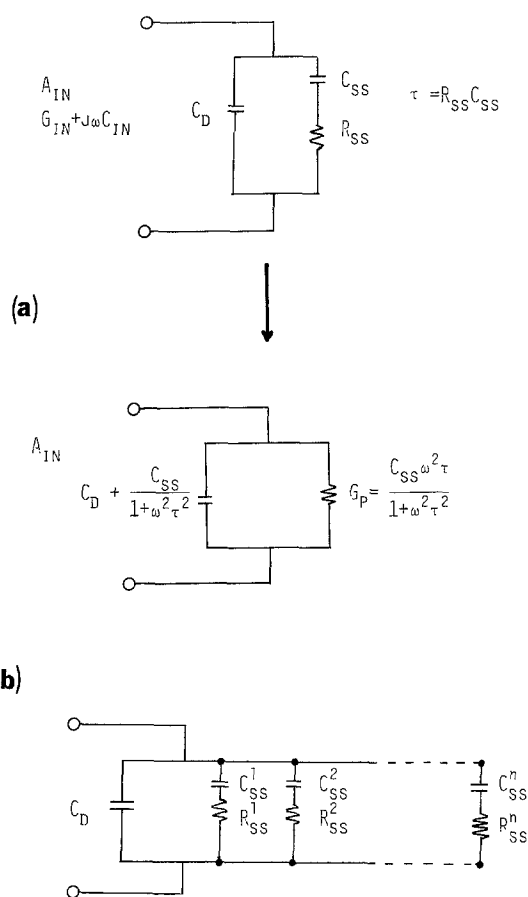


Fig. 1. (a) Equivalent circuit for "single-level" time constant surface states in parallel to the depletion layer capacitance in MOS devices. (b) Equivalent circuit for "multi-level" time constant surface states in parallel to the depletion layer capacitance in MOS devices. Key:  $C_D$ , depletion layer capacitance;  $C_{SS}$ , surface-state capacitance;  $R_{SS}$ , surface-state resistance;  $G_P$ , equivalent parallel conductance of the surface states.

equal to  $2G_P/\omega$ . Hence, the capacitance associated with the surface states can be readily calculated. The density of surface states at a given energy,  $N_{SS}$  (in units of  $eV^{-1} cm^{-2}$ ), can easily be obtained from  $G_P$ , since

$$N_{SS} = 2G_P\tau/e \quad [2]$$

(where  $e$  is the electronic charge). The value of  $\tau$ , assumed to be independent of potential, is taken as that corresponding to the peak value in a plot of  $G_P/\omega$  vs.  $\omega$ .

There have not been many reports on the use of the a-c conductance technique in studies of electrolyte/semiconductor PEC systems (17, 18). Barabash and Cobbold (17) reported some preliminary investigations on the dependence of interface-state properties of electrolyte/SiO<sub>2</sub>/Si structures on pH. Essentially the results parallel those observed for MOS devices and confirm the validity of a-c conductance technique for evaluating interface-state properties of semiconductor/liquid junctions. DuBow and Rajeshwar (18) have reported a systematic study of the admittance characteristics of the n-GaAs/AlCl<sub>3</sub>-butylpyridinium chloride room temperature molten salt interface and demonstrated that the equivalent parallel conductance is more sensitive to interface-state properties than the parallel equivalent capacitance, although both fundamentally contain identical information about the surface-state properties.

We report below the results of a-c impedance technique studies of n-MoTe<sub>2</sub> in MeCN, 0.1M tetra-n-butylammonium perchlorate (TBAP) containing a number of redox couples with widely differing redox potentials. MoTe<sub>2</sub> is a layered compound whose properties as a semiconductor electrode were first studied by

Tributsch and co-workers (19). More recent studies of PEC cells with MoTe<sub>2</sub> are described by Abruna *et al.* (20).

## Experimental

**Crystal growth.**—The  $\alpha$ -MoTe<sub>2</sub> crystals were grown by halogen vapor transport from MoTe<sub>2</sub> powder (Great Western Inorganics, Golden, Colorado, 99.9%) Either Br<sub>2</sub> (70 mg) or TeCl<sub>4</sub> (100 mg) was used as a transporting agent for every 5g of MoTe<sub>2</sub>. These were introduced into a quartz tube (length 19 cm, diameter 18 mm), evacuated to better than  $5 \times 10^{-5}$  Torr, and sealed. Samples using bromine transport were held at liquid nitrogen temperature during evacuation. The sealed tube, with the powder evenly distributed along the length of the tube, was introduced into a horizontal split tube furnace (Hevi-Duty Electric Company, Watertown, Wisconsin; length, 18 in., diameter 1 1/4 in.) and held at a maximum temperature of 875°C. The temperature decreased to around 800°C at the ends of the sample and increased crystal growth could be noticed in these regions. Favorable conditions for crystal growth were ensured when the tube was cooled by convection of air through the split tube furnace, with the majority of the crystals growing on the wall above the original charge. After the transport had proceeded sufficiently, the tube was removed from the furnace and a suitable section was held under running water to condense the vapor phase. The rest of the tube could then be cooled without heavy contamination of the crystals with the transport agent.

Samples transported with bromine required 2-3 days to produce large crystals ( $\sim 50 mm^2$ ), whereas TeCl<sub>4</sub> could transport good crystals in approximately 18 hr. In both cases, an increased concentration of transport agent increased the growth rate; conditions for growth of the best crystals are those given above. Crystals occurred in clusters, away from the side of the tube in the form of platelets of up to 1 cm<sup>2</sup> in area. Some crystals exhibited hexagonal growth spirals and many were twinned. However, a significant fraction had one flat crystal surface, and a few grew as flawless hexagonal plates from one corner. Electron microprobe analysis could not detect the presence of halogens in the transported crystals or any variation in composition between crystals.

**Electrodes.**—Single crystals of  $\alpha$ -MoTe<sub>2</sub> were selected from the clusters of crystals and cut with a razor blade to the desired dimensions. The face  $\perp$  C axis was peeled off with adhesive tape and back-ohmic contacts were made with Ga/In alloy. A copper wire lead for electrical contact was attached to the back-side with silver conductive paint (Allied Product Corporation, New Haven, Connecticut) and was subsequently covered with 5 min epoxy. The assembly was mounted into 7 mm diam glass tubing and held in position with silicone rubber sealant (Dow Corning Corporation, Midland, Michigan) which also served as an effective seal against the seepage of electrolyte solution to the rear of the semiconductor. The exposed area of the electrode was about 0.05 cm<sup>2</sup>. The surface of the electrode was treated prior to use with 6M HCl for 5-10 sec and then rinsed thoroughly with distilled water and dried.

The solvent, acetonitrile (MeCN), was purified and stored as described elsewhere (21). All chemicals, employed after purification or in the purest form commercially available, were dried under vacuum before use. A check of the purity of all chemicals used was performed by cyclic voltammetry at a Pt disk electrode (0.02 cm<sup>2</sup>) at the beginning of each experiment. Polarographic grade tetra-n-butylammonium perchlorate (TBAP), which was twice recrystallized from acetone-ether and dried under a vacuum of  $< 10^{-5}$  Torr for two days, was used as the supporting electrolyte at 0.1M concentration.

A three-compartment electrochemical cell was used. A large area ( $> 40 \text{ cm}^2$ ) Pt gauze counterelectrode immersed in the same compartment as the working electrode was used in impedance measurements. A Pt gauze, separated from the main compartment by a medium porosity glass frit was used as the counterelectrode for coulometric bulk electrolysis. The reference electrode was an aqueous saturated calomel electrode (SCE) with a saturated KCl agar plug, immersed directly in the main compartment. All potentials, unless stated otherwise, are reported vs. this SCE.

A Princeton Applied Research (PAR) Model 173 potentiostat and a PAR Model 175 universal programmer, equipped with a Houston Instruments (Austin, Texas) Model 2000 X-Y recorder were used to obtain cyclic voltammograms. For impedance measurements, a Soltec (Sun Valley, California) Model 6432 X-Y<sub>1</sub>Y<sub>2</sub> recorder was employed. The lock-in amplifier technique, which yields the in-phase ( $0^\circ$ ) and out-of-phase ( $90^\circ$ ) components of a sine wave superimposed onto a linear potential ramp was employed. The a-c signal (12 mV peak-to-peak) at different frequencies was provided by an external signal generator, a Hewlett-Packard (Palo Alto, California) Model 200CD wide range oscillator. Components of the total impedance were obtained with a PAR Model 5204 lock-in amplifier. All solutions were prepared and sealed in a helium-filled Vacuum Atmosphere Corporation (Hawthorne, California) glove box.

### Results

**Capacitance-voltage plots.**—The two important parameters, the flatband potential ( $V_{FB}$ ) and doping density are usually deduced from Mott-Schottky (MS) plots. Such MS plots for n-MoTe<sub>2</sub> in MeCN containing 0.1M TBAP alone are given in Fig. 2 for frequencies in the range 200 Hz-7 kHz. Although there is a very small dispersion in the slope, the  $V_{FB}$  for all plots is located at  $-0.3\text{V vs. SCE}$ . If the dielectric constant of n-MoTe<sub>2</sub> is taken as that of n-MoSe<sub>2</sub> (22), the donor density ( $N_D$ ) is calculated to be about  $2 \times 10^{17} \text{ cm}^{-3}$ . The difference ( $\Delta E_F$ ) between the conduction bandedge (CB) and the Fermi level ( $E_F$ ) can be calculated from the Fermi-Dirac equation (23). With the reduced mass for the electron taken as the rest mass (22),  $\Delta E_F$  is  $\sim 0.1 \text{ eV}$ , so that the conduction bandedge lies at  $-0.4\text{V}$ . With an MoTe<sub>2</sub> bandgap 1.1 eV (24), the valence bandedge is at  $0.7\text{V vs. SCE}$ . The band positions and the formal potentials of the redox couples employed in this study are given in Fig. 3.

**Conductivity.**—The value of the conductivity has been computed from the equation  $\sigma = ne\mu$ , where  $\sigma$  is the conductivity ( $\Omega^{-1} \text{ cm}^{-1}$ ),  $n$  is the charge carrier density ( $\text{cm}^{-3}$ ),  $e$  is the electronic charge ( $1.6 \times 10^{-19} \text{ C}$ ), and  $\mu$  is the mobility ( $\text{cm}^2/\text{V sec}$ ). A value of  $\mu = 20$  is taken from the literature (25). With  $n = 2 \times 10^{17} \text{ cm}^{-3}$ , the resistivity ( $1/\sigma$ ) is found to be  $1.56 \Omega \text{ cm}$ . This is in good agreement with previous values reported (26) for single crystal n-MoTe<sub>2</sub>.

**Impedance measurements.**—The properties of the interface were primarily deduced from a-c impedance measurements. The impedance of the semiconductor/electrolyte interface was measured as a function of both the electrode potential and frequency (or angular frequency,  $\omega$ ). The frequency range studied was 50 Hz-7 kHz. Typical plots of  $G_p$  vs.  $V$  and  $C$  vs.  $V$  are shown in Fig. 4 for n-MoTe<sub>2</sub> in MeCN containing 0.1M TBAP alone. Figure 5 shows similar plots in the presence of various redox couples. As described previously, a plot of  $G_p/\omega$  vs.  $f$  can be employed to determine the time constant of surface states. Such a plot is given in Fig. 6a for MeCN, 0.1M TBAP at  $0.3\text{V vs. SCE}$ . Plots of  $G_p$  vs.  $V$  and  $C$  vs.  $V$  in MeCN in the presence of  $\text{I}^-$  (as TBAP) and both  $\text{I}^-$  and  $\text{I}_3^-$  are shown in Fig. 7 and 8, respectively. For comparison, plots of n-MoTe<sub>2</sub> in

aqueous solutions containing  $\text{I}^-$  and  $\text{I}^-/\text{I}_3^-$  are given in Fig. 9.

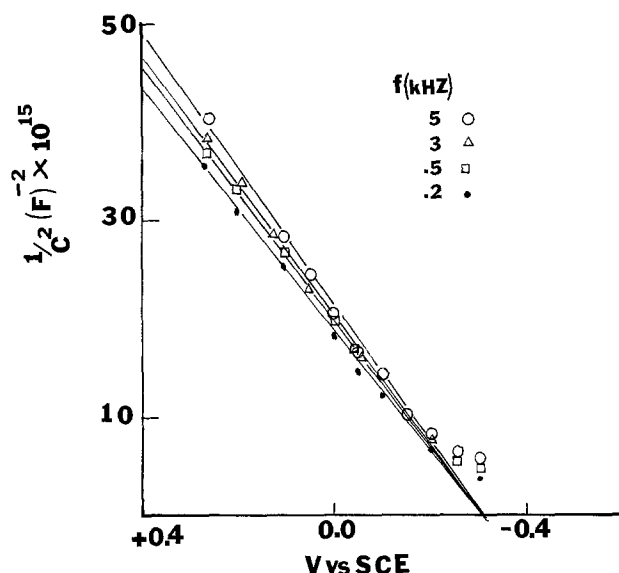


Fig. 2. Mott-Schottky (MS) plots of n-MoTe<sub>2</sub> in MeCN containing 0.1M TBAP alone, at different frequencies.

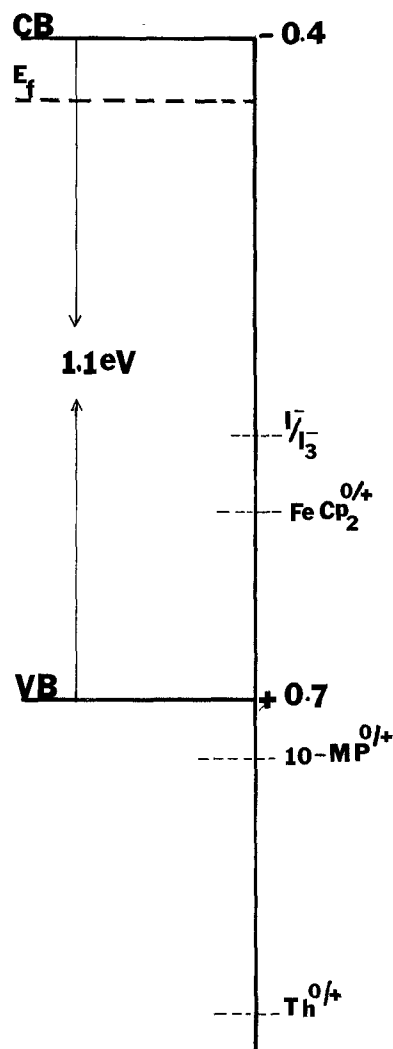


Fig. 3. Position of bandedges of n-MoTe<sub>2</sub> in MeCN containing 0.1M TBAP. CB, conduction bandedge; VB, valence bandedge;  $E_F$ , Fermi level;  $\text{I}^-/\text{I}_3^-$ , iodine;  $\text{FeCp}_2$ , ferrocene; 10-MP, 10-methylphenothiazine; Th, thianthrene.

### Discussion

The presence of surface states can cause frequency dependent slopes and flatband potentials ( $V_{FB}$ ) in MS plots, and the absence of surface states is sometimes assumed when one obtains frequency independent MS plots. Although n-MoTe<sub>2</sub> shows frequency independent MS plots, the in-phase component provides evidence for surface states. The in-phase component of the total impedance has been shown to deal directly with rates of emission and capture of carriers from surface states to either the bandedges or the bulk traps (14a). Consider Fig. 4, where the  $G_p$  vs.  $V$  and  $C$  vs.  $V$  plots are given for n-MoTe<sub>2</sub> in MeCN containing 0.1M TBAP alone. The  $C$ - $V$  plots are frequency independent; however, the plot of  $G_p$  vs.  $V$  shows a hump near +0.3V whose magnitude is frequency dependent. The  $G_p$  values in the depletion region vary with frequency by nearly two orders of magnitude while the overall capacitance values change only marginally in the same frequency regime. This observation, that the equivalent parallel conductance is more sensitive to the presence of surface states than the quadrature component for semiconductor/liquid junctions, parallels that observed in MOS devices (17). Nicollian and Goetzberger (14a) observed that for Si/SiO<sub>2</sub>/M the capacitance increased by only 14% while the in-phase component varied by one order of magnitude for the same frequency domain. Several authors have shown that the surface states located in a particular potential regime may be composed of surface states with different time constants (27). The equivalent circuit for this condition

is shown in Fig. 1b, where several different  $R_i$ - $C_i$  elements are connected in parallel with the space charge layer capacitance. For simplicity, however, we assume that the surface states in n-MoTe<sub>2</sub> can be represented by a single time constant and the equivalent circuit is shown in Fig. 1a. The plot of  $G_p/\omega$  vs.  $f$  for a given potential exhibits a peak at a particular frequency characteristic of the time constant of the surface state (Fig. 6a). The peak value occurs at 3000 Hz, corresponding to a time constant  $\omega^{-1} = (2\pi f)^{-1} = 5 \times 10^{-5}$  sec. This time constant probably represents a weighted average of time constants associated with surface states near 0.3V. The increase in  $G_p/\omega$  at low frequencies suggests that a faradaic component also contributes to the measured total conductance at these frequencies (18). If the 50  $\mu$ sec time constant is taken to represent that associated with surface states at n-MoTe<sub>2</sub>, the density of surface states ( $N_{ss}$ ) can be calculated from Eq. [2]. Figure 6b is a typical plot of  $N_{ss}$  ( $\text{cm}^{-2} \text{eV}^{-1}$ ) for the n-MoTe<sub>2</sub> electrode in MeCN, 0.1M TBAP solution containing FeCp<sub>2</sub><sup>0/+</sup> over the potential range +0.4 to +0.1V vs. SCE, where a peak in the  $G_p$  vs.  $V$  plot occurs. The surface-state density in this potential range varies between  $5 \times 10^{10}$  and  $3 \times 10^{11} \text{ cm}^{-2} \text{eV}^{-1}$ . The time constant indicates that these surface states are fast surface states (28). Integration of  $N_{ss}$  with potential over this region (0.2-0.4V) yields a total surface density,  $N_{ss'}$ , of ca.  $10^{10} \text{ cm}^{-2}$ . Note that this density of surface states is not sufficient for Fermi level pinning to occur (10). This is demonstrated for a 10-methylphenothiazine (10-MP<sup>0/+</sup>) solution (Fig. 5c) whose

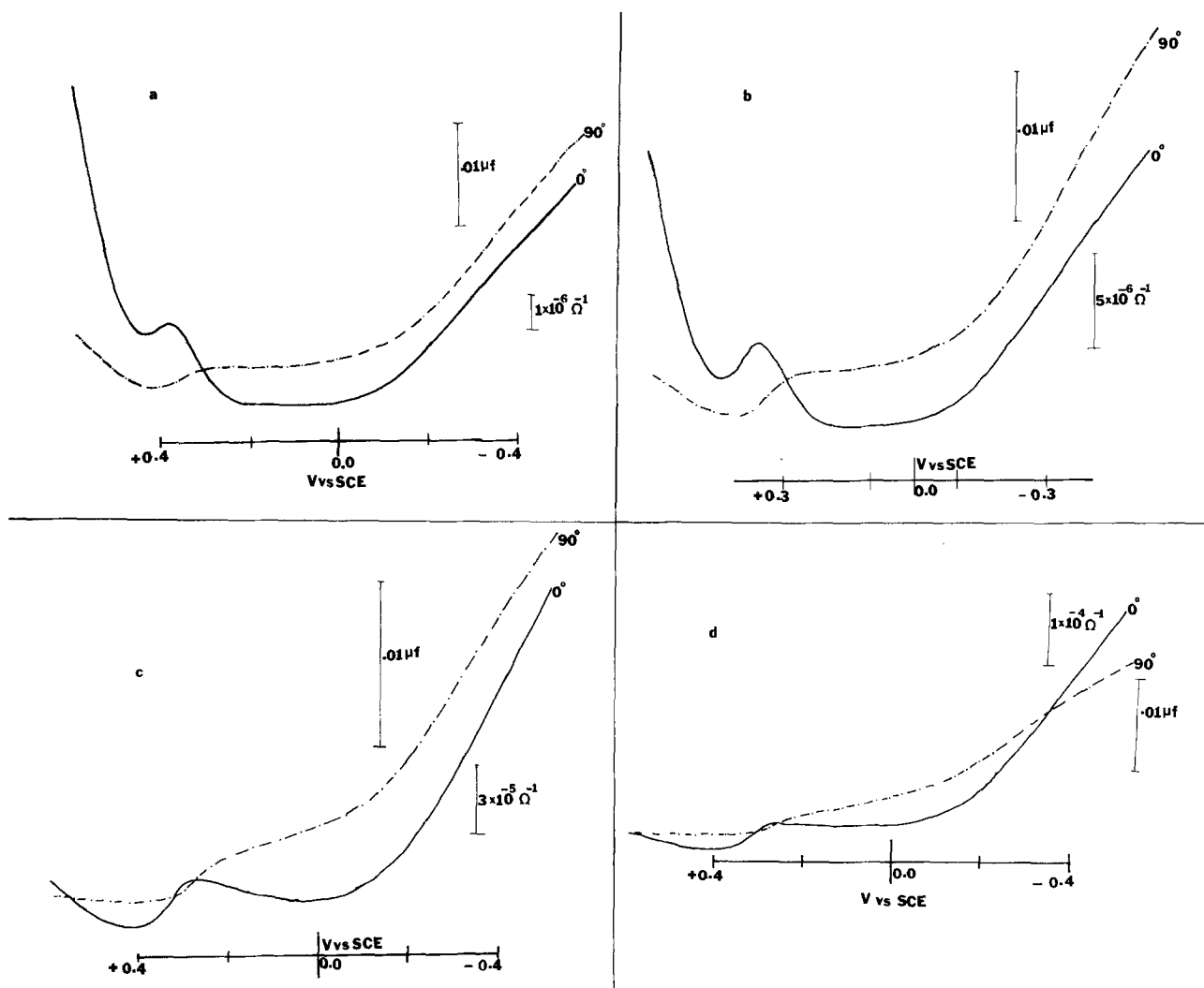


Fig. 4. Parallel equivalent conductance ( $G_p$ ) ( $0^\circ$  component) and capacitance ( $C$ ) ( $90^\circ$  component) vs.  $V$  for n-MoTe<sub>2</sub> in MeCN containing 0.1M TBAP. Frequency ( $f$ ) = (a) 200 Hz; (b) 500 Hz; (c) 3000 Hz; (d) 5000 Hz.

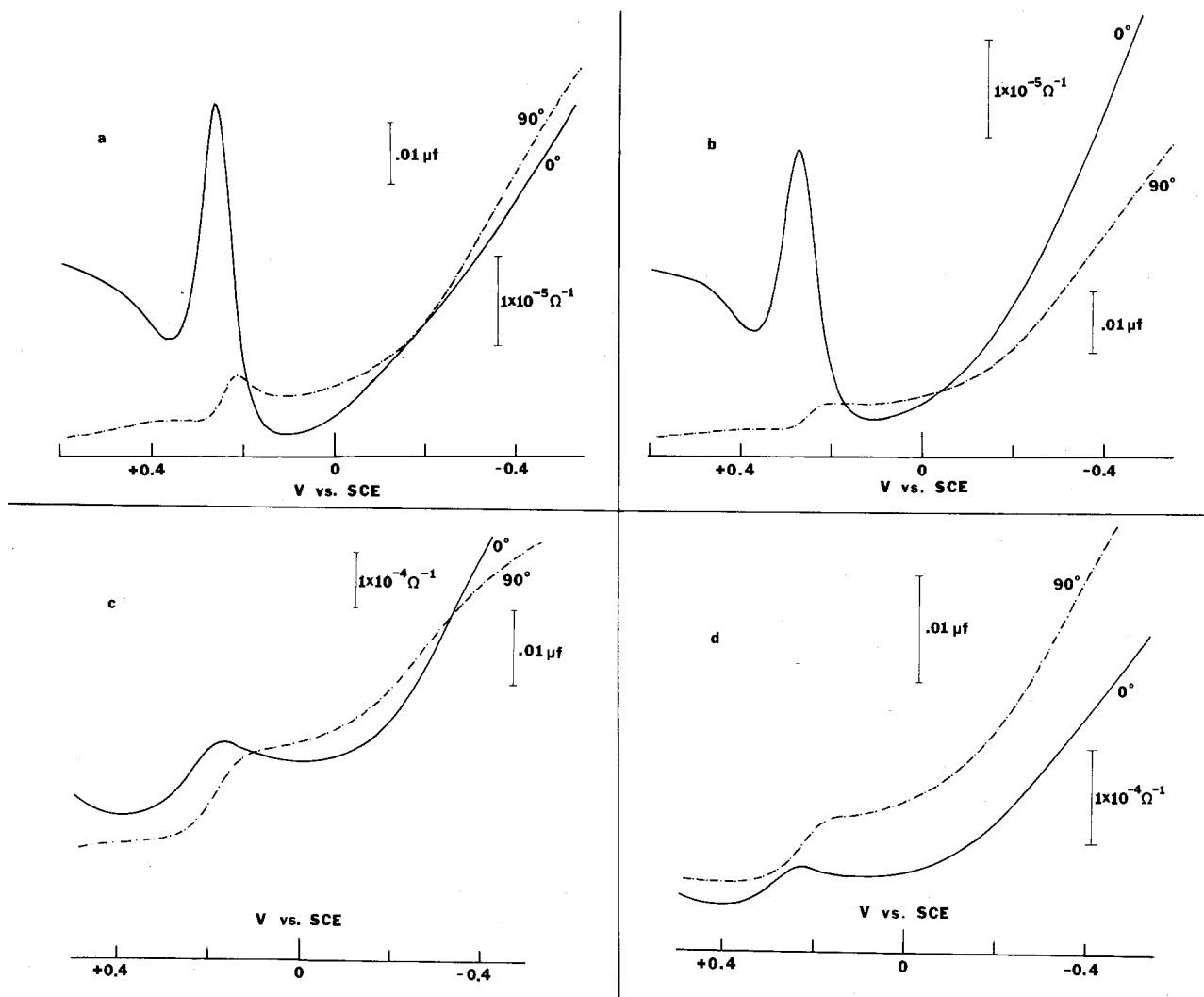


Fig. 5.  $G_p$  and  $C$  vs.  $V$  for  $n\text{-MoTe}_2$  in MeCN, 0.1M TBAP solution containing (a) 10 mM  $\text{FeCp}_2$  and 1.2 mM  $\text{FeCp}_2^+$ ;  $f = 200$  Hz. (b) 10 mM  $\text{FeCp}_2$ ;  $f = 500$  Hz. (c) 10 mM 10-MP and 1 mM  $10\text{-MP}^+$ ;  $f = 2000$  Hz. (d) 8 mM  $\text{Th}^0$ ;  $f = 2000$  Hz.

$V_{\text{redox}}$  is located +0.1V positive of the VB of  $n\text{-MoTe}_2$ . In the presence of  $10\text{-MP}^{0/+}$ , the  $G_p$  vs.  $V$  and  $C$  vs.  $V$  curves are essentially the same as those obtained with blank solution, indicating no change in  $V_{\text{FB}}$ . Addition of other redox couples, such as thianthrene ( $\text{Th}^{0/+}$ ) and  $\text{FeCp}_2^{0/+}$ , also produced no apparent shift in  $V_{\text{FB}}$ . This lack of change in  $V_{\text{FB}}$  for  $n\text{-MoTe}_2$  in the presence of both forms of the redox couple parallels the behavior found for other layered compounds (29). These

results can be contrasted to those of other elemental and compound semiconductors where a monotonic shift of  $V_{\text{FB}}$  with  $V_{\text{redox}}$  in the presence of both forms of the couple in MeCN solution was found (30). This behavior of the layered compounds suggests that surface states are not important in establishing the equilibrium properties of the interface and that specific adsorption of electroactive species on the electrode surface does not occur. Note that the a-c impedance mea-

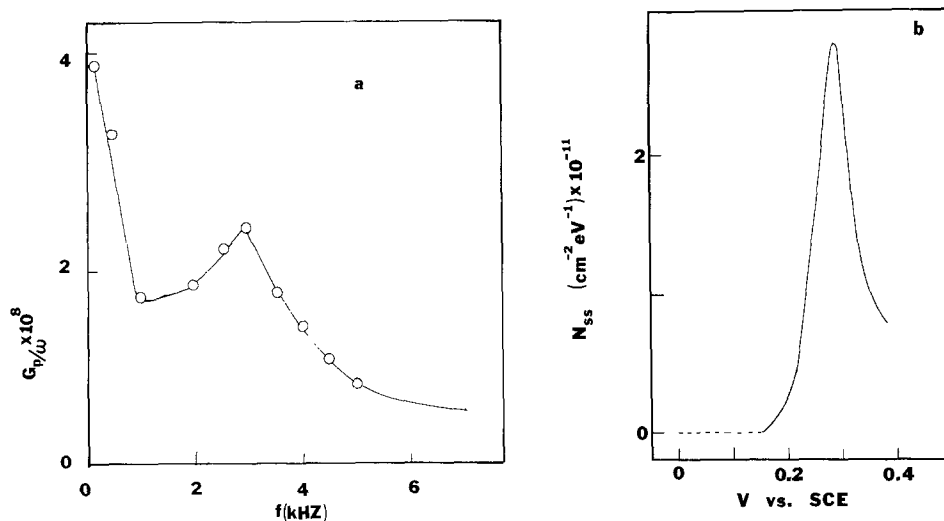


Fig. 6. (a)  $G_p/\omega$  (in  $\text{sec}/\Omega \text{ cm}^2$ ) vs.  $f$  for  $n\text{-MoTe}_2$  in MeCN, 0.1M TBAP solution. Potential: +0.3V vs. SCE. (b)  $N_{\text{ss}}$  vs.  $V$  for  $n\text{-MoTe}_2$  in MeCN, 0.1M TBAP containing  $\text{FeCp}_2^{0/+}$ .

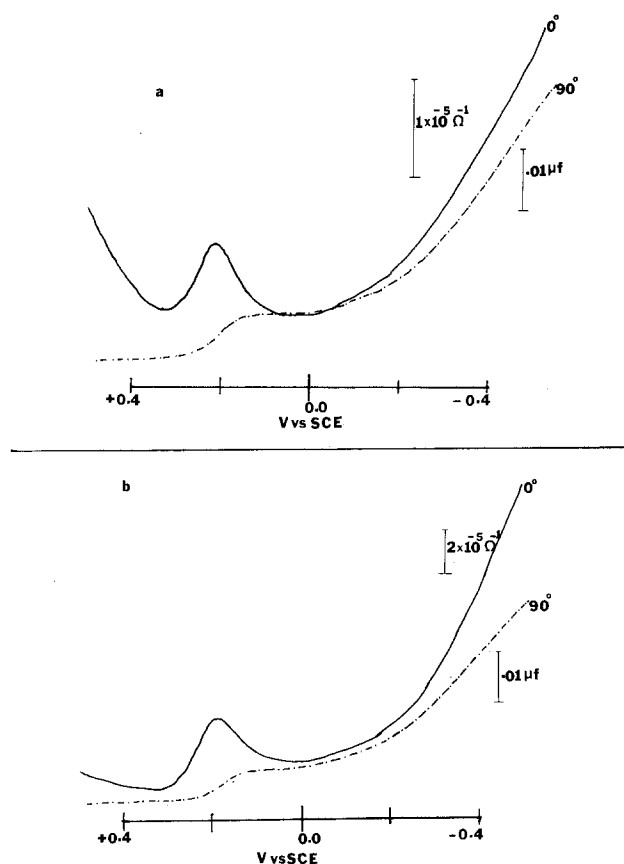


Fig. 7.  $G_p$  and  $C$  vs.  $V$  for  $n\text{-MoTe}_2$  in  $\text{MeCN}$ , 0.1 TBAP solution containing 10 mM  $\text{I}^-$ . (a)  $f = 500$  Hz. (b)  $f = 2000$  Hz.

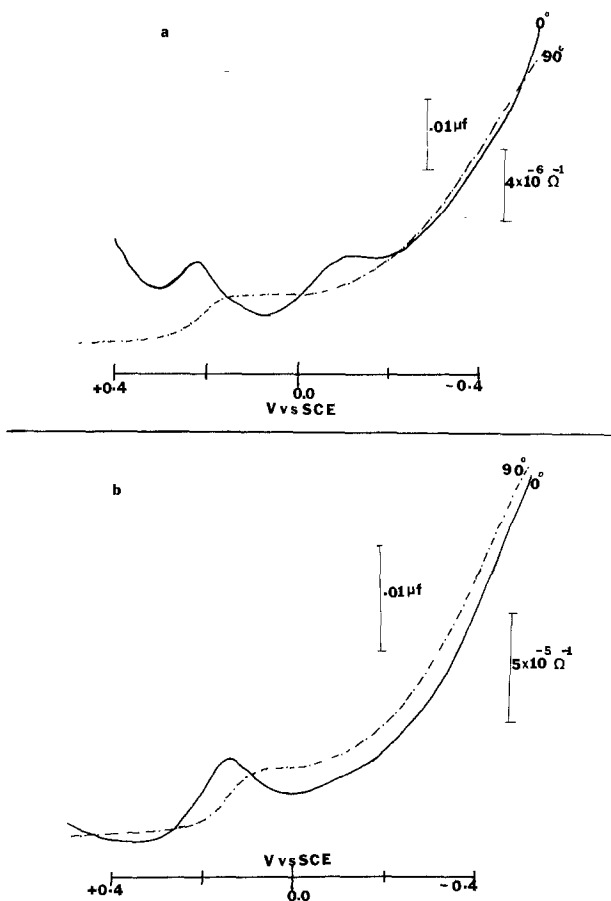


Fig. 8.  $G_p$  and  $C$  vs.  $V$  for  $n\text{-MoTe}_2$  in  $\text{MeCN}/0.1$  TBAP solution containing 10 mM  $\text{I}^-$  and 1.2 mM  $\text{I}_3^-$ . (a)  $f = 200$  Hz. (b)  $f = 2000$  Hz.

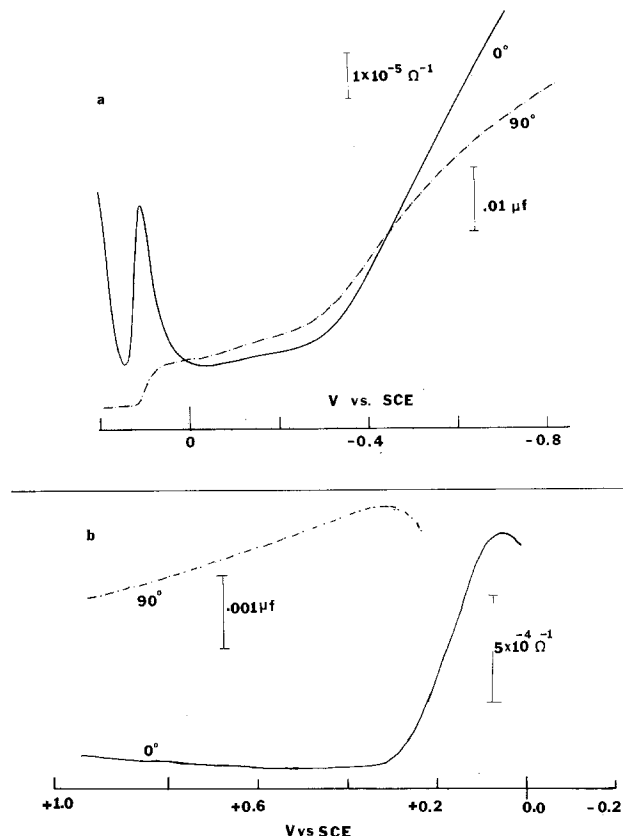


Fig. 9. (a)  $G_p$  and  $C$  vs.  $V$  for  $n\text{-MoTe}_2$  in aqueous solution containing 1M  $\text{KI}$ .  $f = 2000$  Hz. (b)  $G_p$  and  $C$  vs.  $V$  for  $n\text{-MoTe}_2$  in aqueous solution 1M  $\text{KI}/0.1\text{M}$   $\text{I}_2$ .  $f = 2000$  Hz.

measurements carried out in the presence of  $\text{I}^-$  and  $\text{I}^-/\text{I}_3^-$  (Fig. 7 and 8) [iodine has been shown to be specifically chemisorbed on electrode surfaces (31)] indicates no change in the  $G_p$  vs.  $V$  and  $C$  vs.  $V$  plots except for a small hump around  $-0.1\text{V vs. SCE}$  at low frequencies in  $\text{MeCN}$ . This suggests that in  $\text{MeCN}$ ,  $\text{I}^-$  and  $\text{I}_3^-$  are not specifically adsorbed on layered compounds. However, impedance measurements in aqueous solution in the presence of both  $\text{I}^-$  and  $\text{I}^-/\text{I}_3^-$ , shown in Fig. 9a and b, demonstrate that while there is no effect with  $\text{I}^-$  alone, the presence of  $\text{I}_3^-$  shifts  $V_{\text{FB}}$  to more positive values and completely eliminates the humps attributed to the surface states. Kautek and Gerischer (32) reached a similar conclusion for  $\text{MoSe}_2$  in aqueous solutions in the presence of  $\text{I}^-/\text{I}_3^-$ .

## Conclusions

The a-c impedance of the semiconductor/liquid interface parallels that for MOS devices. The in-phase component is more sensitive to surface-state properties than the quadrature component. For  $n\text{-MoTe}_2$  in  $\text{MeCN}$ , the total surface-state density was about  $10^{10}\text{ cm}^{-2}$ , which is too small for Fermi level pinning to occur. The single-level time constant was estimated as  $5 \times 10^{-5}$  sec, which falls in the domain of fast surface states. The behavior of  $n\text{-MoTe}_2$  parallels that of other layered compounds in  $\text{MeCN}$ . While adsorption of  $\text{I}_3^-$  in  $\text{MeCN}$  solutions was not found, shifts of  $V_{\text{FB}}$  in aqueous  $\text{I}_3^-$  solutions suggests interaction of this species with the electrode surface under these conditions.

## Acknowledgments

The support of this research by the National Science Foundation (CHE8000682) and the Solar Energy Research Institute is gratefully acknowledged.

Manuscript submitted April 26, 1982; revised manuscript received ca. Sept. 13, 1982.

Any discussion of this paper will appear in a Discussion Section to be published in the December 1983

JOURNAL. All discussions for the December 1983 Discussion Section should be submitted by Aug. 1, 1983.

Publication costs of this article were assisted by the University of Texas at Austin.

### APPENDIX

The overall equivalent circuit for the semiconductor/solution/metal counterelectrode cell is given in Fig. A-1(a).

Since the counterelectrode area is about 500 times larger than that of the semiconductor electrode, the contribution of the  $C_{\text{counter}}$  and  $R_{\text{counter}}$  to the overall cell impedance can be neglected. Because the electrolyte concentration is fairly high and the bulk resistance of the electrode is small, the contribution of  $C_H$  and  $C_{\text{diff}}$  should be small. The equivalent circuit then reduces to that shown in Fig. A-1(b). Finally, since dark faradaic currents are not observed,  $R_F$  should be very high. Since it is in parallel to  $R_{\text{ss}}$ , the  $R_F$  term can be neglected. Then the equivalent circuit of the semiconductor/liquid junction in the dark reduces to Fig. 1(a). Analysis of the admittance of this circuit,  $A_p$ , where

$$A_p = G_p + j\omega C_p \quad [\text{A-1}]$$

yields the following expressions for the conductance,  $G_p$  (in-phase component) and capacitance,  $C_p$  (quadrature component)

$$G_p = \frac{(\omega C_{\text{ss}})^2 R_{\text{ss}}}{1 + (\omega R_{\text{ss}} C_{\text{ss}})^2} = \frac{\omega^2 C_{\text{ss}} \tau}{1 + (\omega \tau)^2} \quad [\text{A-2}]$$

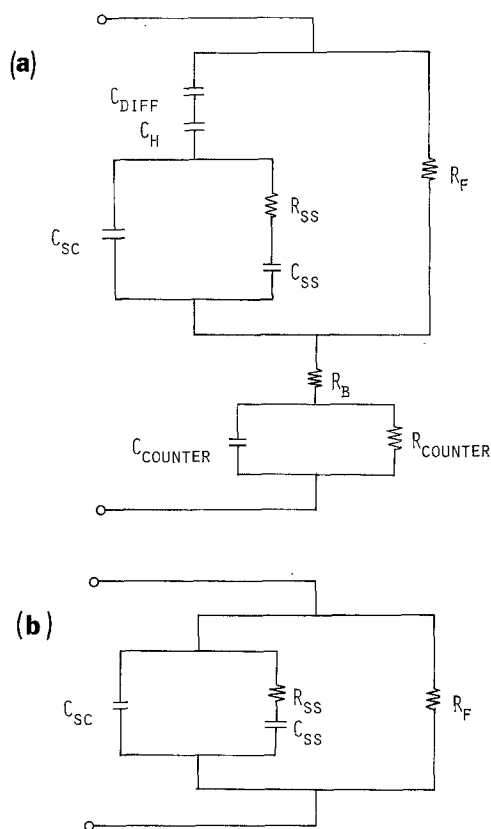


Fig. A-1. Equivalent circuit for the semiconductor/solution/metal counterelectrode cell.  $C_{\text{counter}}$ , capacitance associated with counterelectrode/liquid junction;  $C_{\text{diff}}$ , diffuse layer capacitance;  $C_H$ , Helmholtz layer capacitance;  $C_{\text{sc}}$ , space charge layer capacitance;  $C_{\text{ss}}$ , surface-state capacitance;  $R_B$ , resistance associated with bulk resistance of the electrode and solution resistance;  $R_{\text{counter}}$ , any resistance associated with interface between counterelectrode and solution;  $R_F$ , resistance due to faradaic impedance;  $R_{\text{ss}}$ , resistance arising from the presence of surface states.

$$C_p = C_{\text{sc}} + \frac{C_{\text{ss}}}{1 + (\omega R_{\text{ss}} C_{\text{ss}})^2} = C_{\text{sc}} + \frac{C_{\text{ss}}}{1 + (\omega \tau)^2} \quad [\text{A-3}]$$

where  $\tau = R_{\text{ss}} C_{\text{ss}}$ .

### REFERENCES

1. T. Tamm, *Phys. Z. Sowjetunion*, **1**, 733 (1932).
2. W. Shockley, *Phys. Rev.*, **56**, 317 (1939).
3. J. Bardeen, *ibid.*, **71**, 717 (1947).
4. C. A. Mead and W. G. Spitzer, *Phys. Rev. A*, **134**, 713 (1964).
5. W. G. Spitzer and C. A. Mead, *J. Appl. Phys.*, **34**, 3061 (1963).
6. (a) R. E. Malpas, K. Itaya, and A. J. Bard, *J. Am. Chem. Soc.*, **101**, 2535 (1979); (b) J. N. Chazalviel and T. B. Truong, *J. Electroanal. Chem. Interfacial Electrochem.*, **114**, 299 (1980).
7. A. B. Bocarsly, D. C. Bookbinder, R. N. Dominey, N. S. Lewis, and M. S. Wrighton, *J. Am. Chem. Soc.*, **102**, 3683 (1980).
8. A. Aruchamy and M. S. Wrighton, *J. Phys. Chem.*, **84**, 2848 (1980).
9. F.-R. Fan and A. J. Bard, *J. Am. Chem. Soc.*, **102**, 3677 (1980).
10. A. J. Bard, A. B. Bocarsly, F.-R. Fan, E. G. Walton, and M. S. Wrighton, *ibid.*, **102**, 3671 (1980).
11. (a) J. G. Simmons and L. S. Wei, *Solid-State Electron.*, **17**, 117 (1974); (b) H. A. Mar and J. G. Simmons, *ibid.*, **17**, 131 (1974).
12. J. G. Simmons and G. W. Taylor, *ibid.*, **17**, 125 (1974).
13. G. Declerck, R. Vanoverstraeten, and G. Broux, *ibid.*, **16**, 1451 (1973).
14. (a) E. H. Nicollian and A. Goetzberger, *Bell Syst. Tech. J.*, **46**, 1055 (1967); (b) H. Deuling, E. Klausmann, and A. Goetzberger, *Solid-State Electron.*, **15**, 559 (1972).
15. K. Kobayashi, Y. Aikawa, and M. Sukigara, *Chem. Lett.*, 679 (1981).
16. P. Janietz, R. Weiche, J. Westfahl, R. Landsberg, and R. Dehmlow, *J. Electroanal. Chem. Interfacial Electrochem.*, **106**, 23 (1980).
17. P. R. Barabash and R. S. C. Cobbold, *IEEE Trans. Electron Devices*, ed-29, 102 (1982).
18. J. DuBow and K. Rajeshwar, Final Report, Oct. 1981, submitted to SERI Division, Golden, CO.
19. H. Tributsch, H. Gerischer, C. Clemen, and E. Bucher, *Ber. Bunsenges. Phys. Chem.*, **83**, 655 (1979).
20. H. D. Abruna, G. A. Hope, and A. J. Bard, *This Journal*, **129**, 2224 (1982).
21. G. Nagasubramanian and A. J. Bard, *ibid.*, **128**, 1055 (1981).
22. W. T. Hicks, *ibid.*, **111**, 1058 (1964).
23. G. Nagasubramanian, A. S. Gioda, and A. J. Bard, *ibid.*, **128**, 2158 (1981).
24. A. Lepetit, *J. Phys.*, **26**, 175 (1965).
25. (a) J. A. Wilson and A. D. Yoffe, *Advan. Phys.*, **18**, 193 (1969); (b) A. D. Yoffe, in "Annual Review of Material Science," Vol. 3, R. A. Huggins, Editor, p. 147, Annual Review, Palo Alto (1973).
26. (a) S. Kabashima, *J. Phys. Soc. Jpn.*, **21**, 945 (1966); (b) M. B. Vellinga, R. deJonge, and C. Hass, *J. Solid State Chem.*, **2**, 299 (1970).
27. A. Goetzberger and S. M. Sze, *Appl. Solid State Sci.*, **1**, 153 (1969).
28. A. Goetzberger and S. M. Sze, *ibid.*, **1**, 154 (1969).
29. G. Nagasubramanian, Bob Lee Wheeler, F.-R. Fan, and A. J. Bard, in "Photoelectrochemistry: Fundamental Processes and Measurement Techniques," W. L. Wallace, A. J. Nozik, S. K. Deb, and R. H. Wilson, Editors, Vol. 82-3, pp. 372-380, The Electrochemical Society Softbound Proceedings Series, Pennington, NJ (1982).
30. G. Nagasubramanian, Bob Lee Wheeler, F.-R. Fan, and A. J. Bard, *This Journal*, **129**, 1742 (1982).
31. W. W. Harvey, W. J. LaFleur, and H. C. Gatos, *ibid.*, **102**, 155 (1962) and references therein.
32. W. Kautek and H. Gerischer, *Electrochim. Acta*, **26**, 1771 (1981).